RESEARCH ARTICLE

Check for updates

Azaborahelicene fluorophores derived from four-coordinate *N,C*-boron chelates: synthesis, photophysical and chiroptical properties†

Pablo Vázquez-Domínguez,[a,b] José Francisco Rizo,[a] Jesús F. Arteaga, [ID][c]
Denis Jacquemin, [ID] *[d,e] Ludovic Favereau, [ID] *[f] Abel Ros [ID] *[a] and Uwe Pischel [ID] *[c]

A series of six azaborahelicenes with varying electron-donor substitution at the 4-position of the aryl residue (*i.e.*, naphthyl) or with variable π-extension of the aryl residue (thianthrenyl, anthryl, pyrenyl) was prepared with an efficient and flexible synthetic protocol. These different types of functionalization afforded notably pronounced intramolecular charge-transfer (ICT) character for the dyes with the strongest electron donor substitution (NMe_2) or easiest to oxidize aryl residues, as evidenced by photophysical investigations. These effects also impact the corresponding chiroptical properties of the separated *M*- and *P*-enantiomers, which notably display circularly polarized luminescence (CPL) with dissymmetry factors in the order of magnitude of 10^{-4} to 10^{-3}. Theoretical calculations confirm the optical spectroscopy data and are in agreement with the proposed involvement of ICT processes.

[a]*Institute for Chemical Research (CSIC-US), C/Américo Vespucio 49, E-41092 Seville, Spain. E-mail: abel.ros@iiq.csic.es*
[b]*Department of Organic Chemistry, Innovation Centre in Advanced Chemistry, ORFEO-CINQA, University of Seville, C/Prof. García González 1, 41012 Seville, Spain*
[c]*CIQSO – Center for Research in Sustainable Chemistry and Department of Chemistry, University of Huelva, Campus de El Carmen s/n, E-21071 Huelva, Spain. E-mail: uwe.pischel@diq.uhu.es*
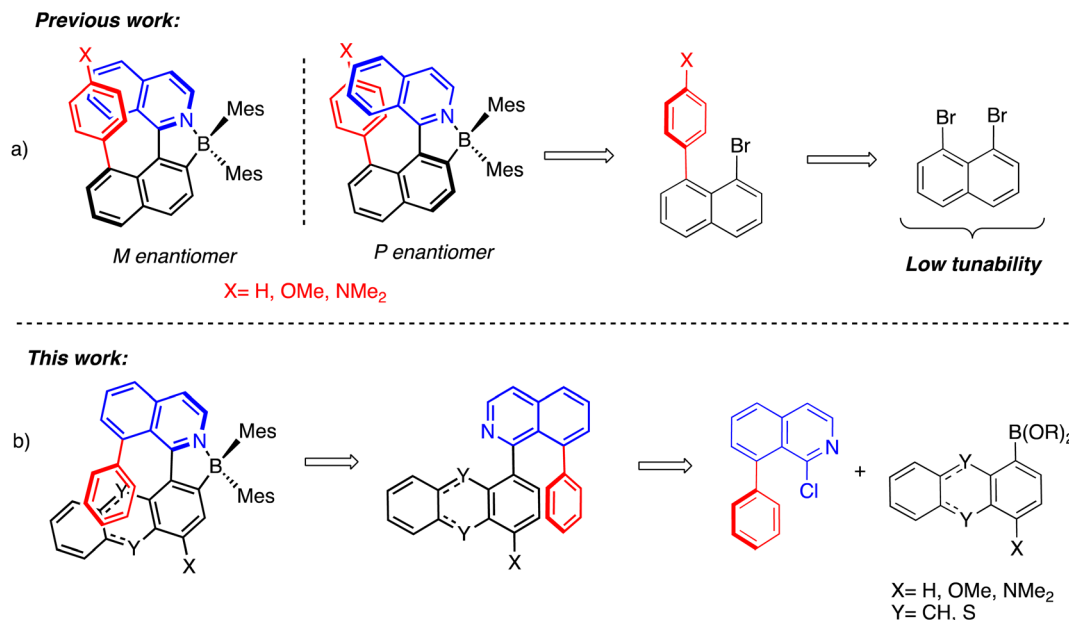[d]*Nantes Université, CNRS, CEISAM UMR 6230, F-44000 Nantes, France. E-mail: Denis.Jacquemin@univ-nantes.fr*
[e]*Institut Universitaire de France (IUF), F-75005 Paris, France*
[f]*Univ Rennes, CNRS, ISCR-UMR 6226, F-35000 Rennes, France. E-mail: ludovic.favereau@univ-rennes1.fr*
†Electronic supplementary information (ESI) available. CCDC 2296415. For ESI and crystallographic data in CIF or other electronic format see DOI: https://doi.org/10.1039/d3qo01762a

Introduction

The design of organic chiral compounds displaying circularly polarized luminescence (CPL) is in the limelight because of their potential in optoelectronic applications, notably organic light-emitting diodes (OLEDs) and CP light detectors, as well as in chiral sensing and bioimaging.[1–7] Currently, significant efforts are directed towards the rationalization of the structural and electronic factors governing both the intensity and sign of CPL in chiral molecules aiming at establishing the molecular design of emitters with high CPL efficiency. The latter aspect is generally quantified using the luminescence dissymmetry factor g_{lum} ($g_{lum} = 2(I_L - I_R)/(I_L + I_R)$), which falls in the 10^{-4}–10^{-2} range for classical "small" organic molecular (SOM) chiral

emitters.[8–12] These values are below the ones obtained for luminescent chiral lanthanide and Cr(III) complexes, *i.e.*, up to 1.4 and 0.3,[1,5,13–15] respectively, chiral polymeric materials[16–23] and other intermolecular approaches involving chiral molecules, such as energy transfer, charge transfer, and excimers.[24–31] However, SOM chiral dyes are attractive because of their tunable optoelectronic properties and their straightforward processability.[16–20,22,23] These aspects, combined with their often high molar extinction coefficient, provide organic chiral dyes with potentially high levels of CPL brightness[32,33] and make them valuable candidates for CPL applications.[20,34–40]

While carbo-[*n*]-helicenes and their derivatives have been an archetypical class of organic chiral systems for developing efficient CPL emitters, the introduction of a B atom with an empty p_z-orbital as a functional group on chiral π-conjugated systems, or within the helical molecular systems has been shown to be an ingenious way of tuning the resulting chiral optoelectornic properties.[41–53] In another approach, the B atom has also been used as an anchoring unit for a chiral ligand, such as 1,1′-bi(2-naphthol) (BINOL) and its derivatives, on boron dipyrromethene (BODIPY) dyes, affording a simple and efficient way of obtaining new CPL emitters.[54–57]

Our recent contributions in this research area focused on CPL-active four-coordinate *N,C* chelate organoboranes (Fig. 1a),[58] showing significant emission (Φ_f up to 0.3) and CPL with dissymmetry factors as large as 3.5×10^{-3}. Despite these interesting chiroptical properties, these chiral organoboranes showed low structural tunability, and therefore, we decided to develop a more versatile family of helically chiral

This journal is © the Partner Organisations 2024

*Org. Chem. Front.*, 2024, **11**, 843–853 | **843**

Fig. 1 (a) Our previously described CPL-active azaborahelicene systems. (b) Retrosynthetic route for the new family of azaborahelicenes described in this study.

N,C-boranes (Fig. 1b), enabling us modifying their optoelectronic properties. Especially the electron-donating properties of the aryl residue are expected to modulate the intramolecular charge-transfer (ICT) character of the excited state and hence, the chiroptical properties of the herein investigated dyes.[59,60] In previous works on the dye platform we have shown that more pronounced ICT character leads to reduced intersystem crossing.[60] In addition a reduced conformational flexibility may hinder other non-radiative deactivation channels, such as internal conversion. Both of these characteristics would in principle contribute to increased radiative deactivation of excited states, thereby enhancing the possibility to observe significant CPL.

Results and discussion

Synthesis

The synthesis of the target dyes (see Schemes 1 and 2) employs the arylisoquinolines **3a–f** as precursors. The latter are subsequently converted into the corresponding bromide derivatives **4a–f** and finally transformed into the borylated dyes **5a–f**. Thus, starting from 8-phenylisoquinoline, the key 1-chloro-8-phenylisoquinoline building block **1** was obtained in a gram scale following previously described procedures (Scheme 1).[61,62] The Suzuki coupling of **1** with the naphthalene-derived boronic acid derivatives **2a–c** afforded the desired triaryl systems **3a–c** in 72–84% yields (Scheme 1). **3b** and **3c** contain a methoxy or *N,N*-dimethylamino substitutent, respectively, which provide a substantial modification of the electron-donor strength and consequently of the photo-induced ICT process (see below).[59] The coupling reaction was also extended
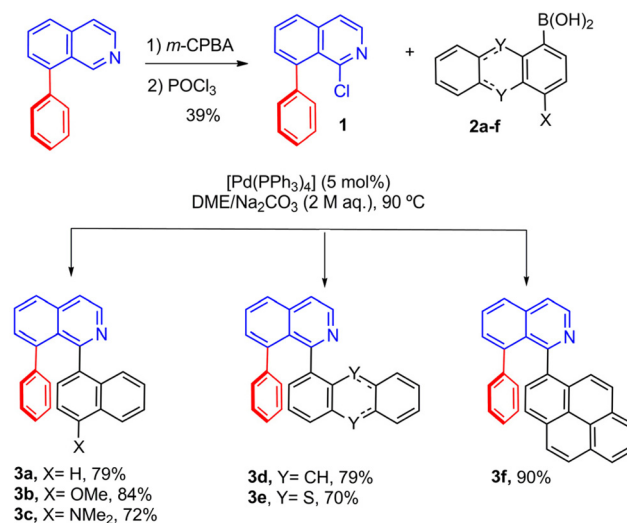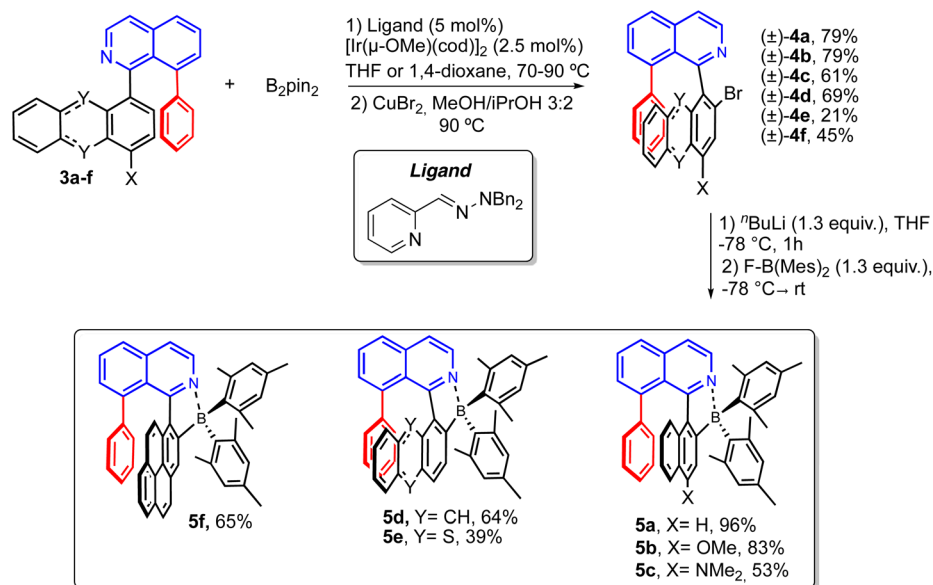

Scheme 1 Synthesis of the arylisoquinolines **3a–f**.

to other electron-rich and extended π-conjugated fragments such as anthryl, thianthrenyl, and pyrenyl, to obtain the corresponding products **3d–f** in 70–90% yields (Scheme 1).

Then, our previously described C–H borylation/bromination methodology was applied to the triaryl systems (Scheme 2),[48,59,63,64] affording the corresponding bromides **4a–f** as racemic mixtures in 21–79% yields. In the case of (±)-**4f**, the moderate yield is partially caused by the formation of *ca.* 20% of a dibrominated product. Finally, the racemic bromides (±)-**4a–f** were subjected to lithiation/borylation conditions to afford the desired fluorescent *N,C*-organoborane dyes (±)-**5a–f** in 39–96% yield. The *M*- and *P*-enantiomers of

844 | *Org. Chem. Front.*, 2024, **11**, 843–853

This journal is © the Partner Organisations 2024

Scheme 2 Synthesis of the dyes **5a–f**.

each dye were obtained by semipreparative chiral HPLC separation with ee values of up to 99% (see the ESI† for details). Their absolute configuration was assigned by comparison of their ECD responses with those of previously published related dyes,[58] and further confirmed by theoretical calculations (see below). All products were characterized by ^{1}H, ^{13}C, and ^{11}B NMR spectroscopy and high-resolution mass spectrometry (see the ESI† for details). The ^{11}B NMR signal at 5.3–5.9 ppm confirms the four-coordinate nature of the boron center for all herein investigated dyes.

X-ray quality crystals of racemic (±)-**5e** were obtained by slow evaporation of a solution of the dye in dichloromethane/hexane. The X-ray structure analysis shows the helicoidal geometry of the dye (Fig. 2), with the thianthrenyl fragment adopting a bent disposition to avoid the steric repulsion with the phenyl substituent. However, although the X-ray picture shows a fixed conformation of the molecule, a rapid interconversion of conformers by dynamic folding along the S···S axis can take place in solution, as reported by others[65,66] and further supported herein by theoretical calculations (see below).

UV/vis-absorption and fluorescence properties

The photophysical properties of the racemic dyes **5a–f** in organic solvents (toluene, dichloromethane, and acetonitrile) are compiled in Table 1 and representative spectra of **5a–c** in toluene are shown in Fig. 3 (see the ESI† for additional spectra related to the other dyes and solvents). Given their electronically diverse structure, the photophysical and chiroptical properties of the dyes are discussed by following two main aspects: (a) the influence of electron-donor substitution X at the 4-position of the naphthalene moiety for **5a–c** and (b) the degree of π-conjugation of the aryl residue in the dyes **5a** and **5d–f**.

For **5a–c** there is a clear trend of a bathochromic shift on moving from **5a** (R = H) to **5c** (R = NMe₂), *e.g.*, $\Delta\lambda_{abs}$ = 50 nm
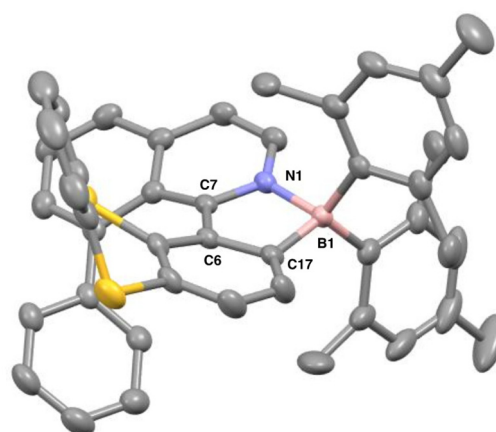
Fig. 2 ORTEP diagram of the crystal structure of dye (±)-**5e** (CCDC 2296415†). The displacement ellipsoids are drawn at 50% probability. Hydrogen atoms are omitted for clarity. Selected bond lengths [Å] and angles [°]: N1–B1 1.652(4), C17–B1 1.632(4), N1–C7–C6–C17 18.3. Although only the *M*-**5e** enantiomer is displayed, the unit cell contains both enantiomers (see CIF file in CCDC).

and $\Delta\lambda_F$ = 80 nm, in toluene. The shift of the emission maximum is even more pronounced in the more polar acetonitrile ($\Delta\lambda_F$ = 121 nm). These observations are an indication that an ICT transition is present.[59,60,67] While this holds for dye **5c**, the emission properties of the dyes **5a** and **5b** are practically insensitive to the solvent polarity. This trend is in line with the electrochemical study of these compounds, which shows a strong decrease for the first oxidation potential of **5c** (E_{ox} = +0.56 *versus* SCE) in comparison to **5a** and **5b** (E_{ox} = +1.10 and 0.94 *versus* SCE, respectively), owing to the presence of the dimethylamino electron donor group (see ESI† for details).

This journal is © the Partner Organisations 2024

Org. Chem. Front., 2024, **11**, 843–853 | **845**

Table 1 Photophysical and chiroptical properties of the dyes **5a–f** in various organic solvents

	$\lambda_{abs}{}^a$ (nm) [ε (M^{-1} cm^{-1})]	$\lambda_F{}^b$ (nm)	Φ_F	$\tau_F{}^c$ (ns)	$\|g_{abs}\| \times 10^{-3\,d}$	$\|g_{lum}\| \times 10^{-3\,e}$
Toluene						
5a	428 [10 000]	504	0.09	2.13		1.7 (495)
5b	465 [9500]	521	0.24	3.98		0.7 (506)
5c	478 [15 000]	586	0.40	8.40		0.1 (550)
5d	492 [8000]	534	0.10	2.18		1.0 (540)
5e^f	382					
5f	448 [20 000]	521	0.22	3.12		0.1 (510)
Dichloromethane						
5a	424 [10 000]	503	0.14	2.74	1.7 (429)	1.0 (503)
5b	434 [9000]	521	0.28	5.54	1.2 (448)	0.7 (521)
5c	475 [11 000]	599	0.39	9.71	0.7 (474)	0.1 (599)
5d	484 [8000]	545	0.09	2.04	1.2 (472)	1.0 (545)
5e^f	380				2.8 (383)	
5f	443 [16 000]	530	0.21	3.36	1.2 (448)	~0
Acetonitrile						
5a	420 [9000]	503	0.07	2.55		1.2 (500) 1.0 (615)
5b	439 [10 000]	524	0.26	5.46		0.5 (520)
5c	467 [13 000]	624	0.18	5.98		~0
5d	465 [6500]	560	0.05	2.82^g		1.1 (555)
5e^f	383					
5f	438 [17 000]	540	0.17	4.01		~0

^{a} Maximum of the longest-wavelength absorption band. ^{b} Maximum of the fluorescence spectrum. ^{c} Fluorescence lifetime; the value of the major component (≥94% weighted contribution) is shown, except for **5d** in acetonitrile. The complete decays and data fits are shown in the ESI.† ^{d} In parenthesis the maximum of the longest-wavelength signal is given. ^{e} The maximum of g_{lum} is given at the wavelength (in parentheses) corresponding to the maximum of the emission signal. ^{f} The low solubility, accompanied by aggregation phenomena, hampered the determination of molar absorption coefficients. Likewise, the fluorescence emission is too weak to allow the safe determination of corresponding photophysical data. ^{g} Multiexponential decay; the intensity-weighted average lifetime is given. The complete decay and data fit is shown in the ESI.†
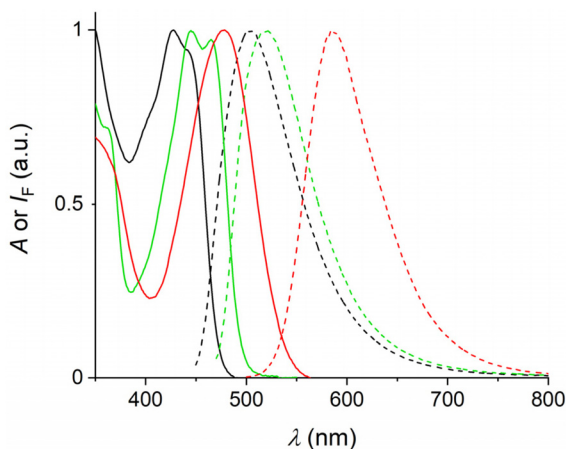
Fig. 3 UV/vis absorption (full lines) and fluorescence spectra (dashed lines) of **5a** (black), **5b** (green), and **5c** (red) in air-equilibrated toluene (dye concentration 20 μM).
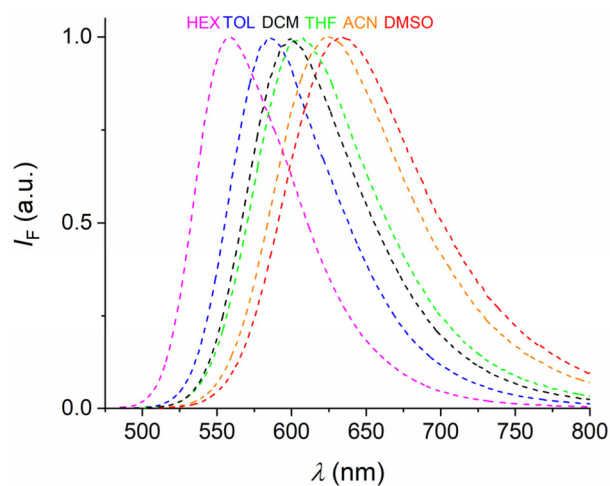
Fig. 4 Fluorescence spectra of dye **5c** in various solvents (dye concentration *ca.* 20 μM, air-equilibrated solutions).

624 nm); see also Fig. 4 for a larger set of solvents of varying polarity. Despite the rather low-lying emissive states, the fluorescence quantum yields remain rather appreciable, reaching values of 0.40 in toluene and 0.18 in acetonitrile. The slight drop in acetonitrile likely relates to the significant non-radiative excited-state deactivations (*cf.* energy-gap law).

The variation of the π-conjugation of the attached aryl residue in the dyes **5a** and **5d–f** has significant effects on their photophysical properties. The longest-wavelength absorption maxima of the dyes are bathochromically shifted in the **5e** < **5a** < **5f** < **5d** order, a ranking holding in all investigated solvents (see Table 1). This corresponds to the increasing π-conjugation in the aryl moiety. This ranking also applies to the fluorescence maxima for the dyes **5a**, **5f**, and **5d**. The effect of the solvent polarity is most notable for the two dyes with the most extended π-conjugation in the aryl residue, *i.e.*, **5d** and **5f**. On changing from *n*-hexane to DMSO a red-shift by *ca.* 22–24 nm was noted for both compounds. As the anthryl and pyrenyl moieties in these dyes have a comparably low oxidation potential, excited state ICT phenomena can be used to rationalize the observed solvent dependence. While dye **5d** has fluorescence quantum yields between 0.05 and 0.10 (depending on the solvent), dye **5f** reaches values of about 0.2 for this parameter. This qualifies both dyes as moderately but significantly fluorescent. Noteworthy, dye **5e** shows too weak fluorescence to be reliably measured, which may be traced back to aggregation-induced quenching and dominant nonradiative de-excitation of rather low-lying excited states (see theoretical calculations below).

The dyes show fluorescence decays (see ESI†) with a dominant lifetime component (≥94%) in the range of 2–4 ns, except for **5c**, which shows somewhat longer lifetimes between 6 ns and 10 ns, depending on the solvent (see Table 1). Dye **5d** in acetonitrile is another exception, because two relatively short components were detected (see ESI†). However, in frozen 2-methyltetrahydrofuran glass at 77 K one dominant short

Focusing on the dye **5c** it is noteworthy that in nonpolar toluene an orange emission is observed (λ_F = 586 nm), while in polar acetonitrile the dye emits in the deep red region (λ_F =

846 | *Org. Chem. Front.*, 2024, **11**, 843–853

This journal is © the Partner Organisations 2024

component (3.4 ns) with a weighted contribution of 96% persists (see ESI†). Although the solvent system is different, this may hint on conformational equilibria at room temperature, leading to a lifetime distribution in this specific case. With the lifetimes and the fluorescence quantum yields, the radiative (k_f) and non-radiative deactivation rate constants (k_{nr}) were estimated. They were found to be in the order of magnitude of 10^7 s^{-1} and 10^8 s^{-1}, respectively (see data in ESI†).

Chiroptical properties

The chiroptical properties were determined for the separated M and P enantiomers. The absolute configuration of the reported chiral emitters was assigned by comparison of the experimental ECD spectra with our previous studies of related azaborahelicences,[58] and further confirmed by Time-Dependent Density Functional Theory (TD-DFT) calculations performed in dichloromethane with the Polarizable Continuum Model (PCM), see the ESI† for further details. Accordingly, the first and second HPLC fractions of compounds **5** correspond to the M- and P-enantiomers, respectively (see the ESI† for details).

As depicted in Fig. 5, each couple of enantiomers displays expected mirror-image ECD spectra, which for dyes M-**5a** and M-**5b** appear rather similar, implying a low-energy negative broad band between 370 and 470 nm (-10 M^{-1} cm^{-1}), followed by a set of positive and negative signals at 350 and 305 nm, respectively, in addition to a positive exciton couplet around 280 nm ($\Delta\varepsilon \sim +60$ M^{-1} cm^{-1}). For these derivatives, the substituent on the naphthyl core seems to have limited impact on the overall ECD responses, as also illustrated when comparing the responses below 250 nm when recorded in acetonitrile (see ESI† for details). However, moving to the more electron-rich amino unit on M-**5c** decreases the overall intensity of the ECD response and induces a change of the high-energy bisignate response at 290 nm.

This change is mainly observed for the latter compound since the ECD of the anthracene, pyrene and thianthrene derivatives, M-**5d**, M-**5f** and M-**5e**, respectively, display a rather similar ECD pattern as M-**5a** with however, a different distribution of relative intensities for the spectrum of M-**5f** due to the intense transitions of the pyrene core. Finally, all investigated dyes display dissymmetry factors $|g_{abs}|$ of *ca.* $(1–3) \times 10^{-3}$ for the lowest energy transition (see Table 1).

The CPL of these new chiral emitters was recorded in solvents of varying polarity, including toluene, dichloromethane, and acetonitrile. Despite their clear ECD responses for the lowest-energy band, the radiative de-excitation of the related excited states does not lead to intense CPL responses. For instance, the enantiomers M-**5a**, M-**5b**, and M-**5d** display negative CPL spectra with maxima corresponding to those of their respective unpolarized fluorescence emission and g_{lum} values of -1.5×10^{-3}, -0.6×10^{-3}, and -1.0×10^{-3}, respectively (Fig. 6). The latter are consistent with the absorption dissymmetry factors g_{abs}, measured at the lowest energy transition (Table 1),[68] indicating that both ground state and emitting excited state have a similar chiral geometry. In contrast, the compound **5c**, which shows a more important ICT character for the emitting excited state, displayed very weak CPL signals
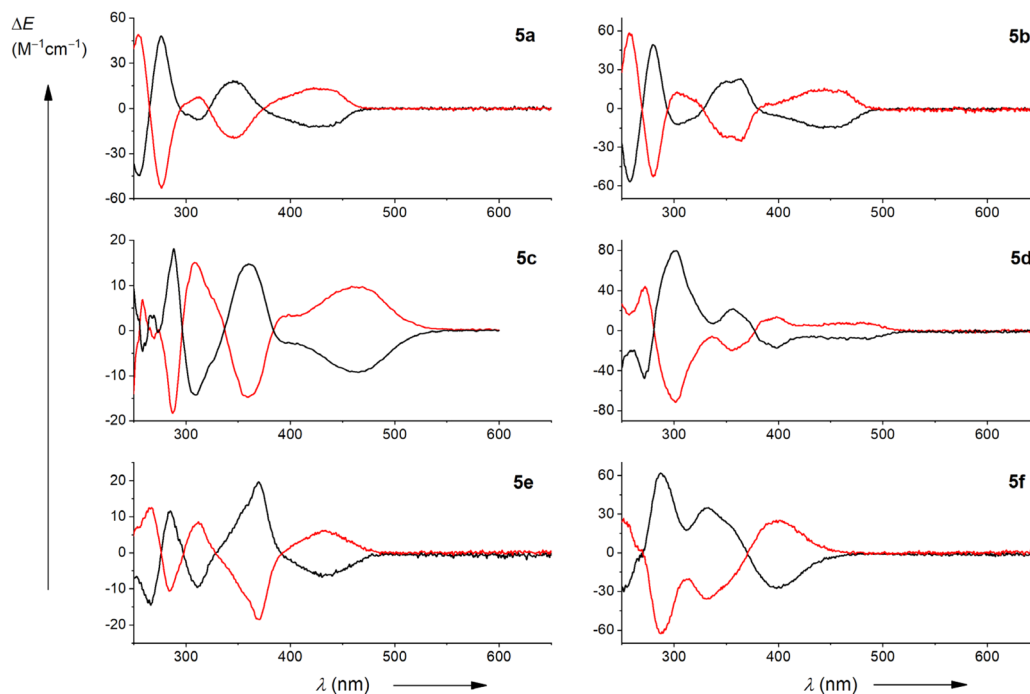
Fig. 5 ECD spectra of the dyes **5a–f** in dichloromethane (dye concentration *ca.* 1 μM; air-equilibrated solutions). The black spectra correspond to the M-enantiomers and the red spectra to the P-enantiomers.

This journal is © the Partner Organisations 2024

Org. Chem. Front., 2024, **11**, 843–853 | **847**
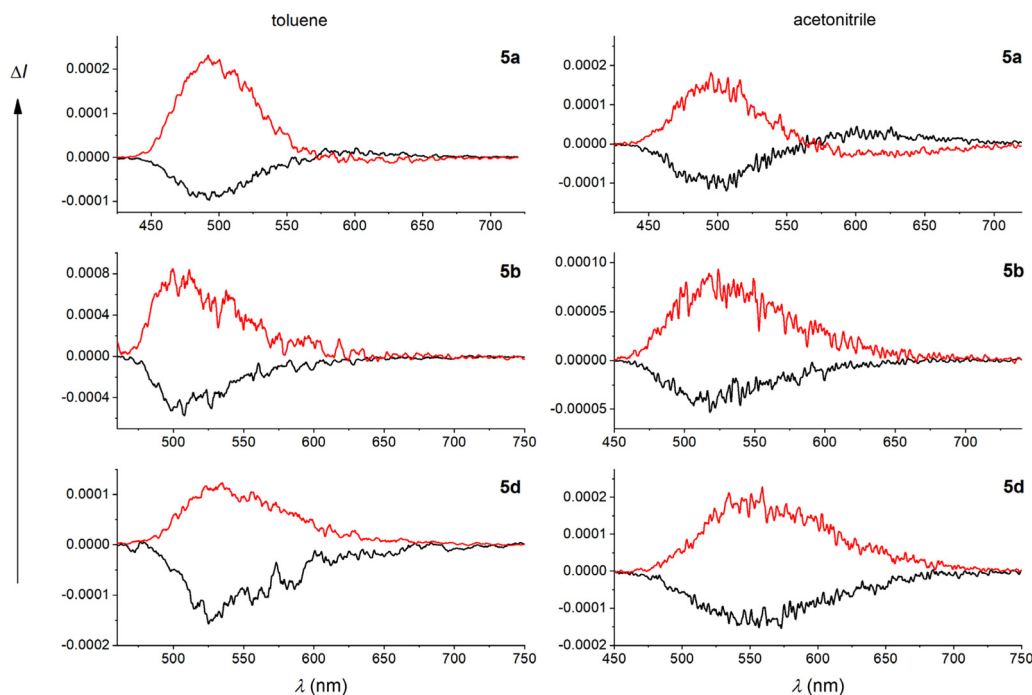
Fig. 6 CPL spectra of the dyes **5a**, **5b**, and **5d** in toluene and in acetonitrile (dye concentration *ca.* 1 μM; air-equilibrated solutions). The black spectra correspond to the *M*-enantiomers and the red spectra to the *P*-enantiomers.

for both enantiomers with $|g_{lum}|$ values of about 1×10^{-4} in toluene, and no reliable responses in acetonitrile. Interestingly, these overall CPL results show the opposite trend to what we observed in our recent study of related borylated arylisoquinoline CPL dyes,[58] for which the chiral emitter with the highest ICT displayed the most intense CPL emission intensity. This comparison clearly highlights the influence of the substituent position on the photophysical and chiroptical properties of the azabora[5]helicene building block. The CPL signals of **5e** and **5f** are too weak to be detected, except for **5f** in toluene. For the former dye this is easily traced back to the already very low unpolarized fluorescence (see above).

Theoretical calculations

To obtain additional insights, we have used theoretical calculations relying on TD-DFT and CC2 approaches (see the ESI† for details). In Fig. 7 the Electron Density Difference (EDD) plots corresponding to the S_0–S_1 absorption for all compounds are shown with the intention to probe the nature of the lowest-lying excited state. One clearly notices the highly-delocalized ICT nature of the involved transitions, where the "lower part" of the compound acts as the donor (mostly in blue) whereas the "top part" takes the role of the acceptor (mostly in red). This effect is particularly pronounced for **5c** in which the donating character of the amino group clearly appears. This latter aspect is consistent with the strong solvatofluorochromism that is observed for this compound (Fig. 4).

Next, we have also simulated the UV/vis-absorption and ECD spectra on the basis of vertical TD-DFT results. The calcu-

lated spectra are displayed in the ESI† and agree well with the experimental ones, though such comparisons that do not account for vibronic couplings always remain qualitative.[69] Indeed, the trend observed for dyes **5a–c** regarding the bathochromic shift of the absorption spectra when increasing the donor strength of the substituent is clearly reproduced, as well as the most intense low energy absorption band at 420 nm observed for the pyrene compound **5f**. The theoretical ECD spectra, calculated for the *M*-enantiomer, are also in line with the recorded ones, and confirm the assignment of the *P* and *M* configuration for the isolated enantiopure compounds.

Finally, as we are well aware of the limits of TD-DFT for many boron-containing systems,[70] we have used a more refined approach including CC2 corrections and allowing the determination of 0–0 energies accounting for state-specific solvation effects. In this way we obtained the following best estimates of the vertical absorption (fluorescence): 438 (512) nm for **5a**, 458 (537) nm for **5b**, 496 (618) nm for **5c**, 488 (579) nm for **5d**, 470 (844/711) nm for **5e**, and 480 (568) nm for **5f**. In the **5a–c** series the results are in good agreement with experimental data, and more importantly with the observed trends. The same holds for **5d** and **5f** with errors in the acceptable range for such comparisons. **5e** is indeed a specific case with two conformers which will be discussed below. For the 0–0 energies, that allow well-grounded comparisons with the experiment, the theoretical (experimental) values are 2.38 (2.69), 2.31 (2.59), 2.04 (2.34), 2.08 (2.42), and 2.07 (2.56 eV) for **5a**, **5b**, **5c**, **5d**, and **5f**, respectively. Note the virtual absence of emission for **5e** hampered the measurement of the 0–0 energy
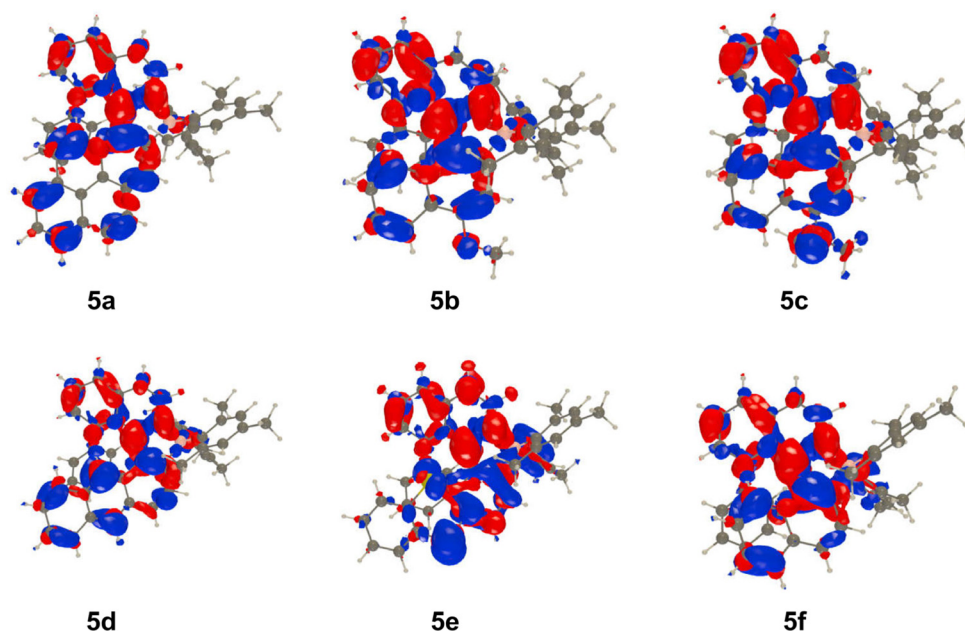
Fig. 7 EDD plots for the dyes **5a–f**. The blue and red lobes represent the decrease and increase of electron density upon absorption, respectively. Contour: 1×10^{-3} a.u.

in this case. The theoretical calculations yield a systematic red-shift, by −0.34 eV on average, which is an acceptable yet significant error for this level of theory.

For compound **5e** we could identify two conformers in the ground electronic state (see Fig. 8), depending on the direction of the out-of-plane deformation of the thianthrene moiety. The second conformer, displayed at the bottom left of Fig. 8, resembles the X-ray crystal structure shown in Fig. 2. Interestingly, the two structures have almost the same energy according to the calculations (we compute a difference smaller

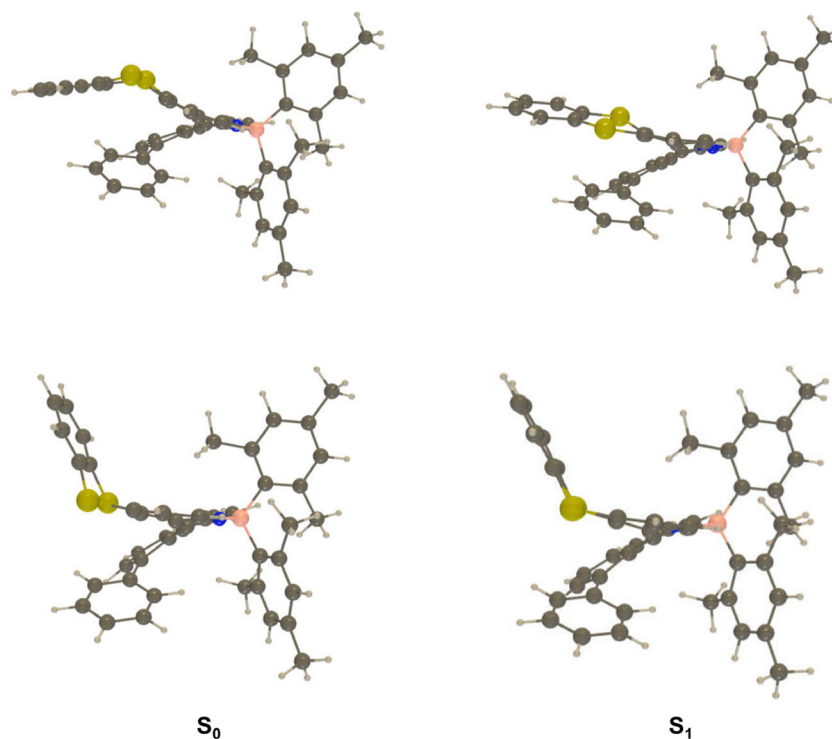
Fig. 8 Representation of the optimal geometries of the two optimized conformers of **5e** in the ground (left) and excited states (right).

This journal is © the Partner Organisations 2024

Org. Chem. Front., 2024, **11**, 843–853 | **849**

than 1 kcal mol^{-1}, *i.e.*, smaller than the typical PCM-DFT error bar), and are likely to co-exist in solution. In the excited state, we also found two conformers, one in which the thianthrene unit is almost becoming planar (top right in Fig. 8), and another still kinked, the former being more stable by 2.6 kcal mol^{-1} on the free energy scale. The planar conformer has a vertical fluorescence wavelength of 844 nm and the kinked, less stable, conformer shows a vertical emission at 710 nm. The presence of two conformers suggests a dynamic excited-state behavior, which combined with energy gaps smaller than 2 eV is detrimental for emission. This is in agreement with the experimental observation of the essentially non-fluorescent nature of **5e**. The relative balance between the two species might also change with the solvent and the experimental conditions, explaining the difficulty to obtain reliable measurements for the emission.

Conclusions

The family of fluorescent borylated arylisoquinolines can be extended toward optically active dyes with helical chirality. A flexible synthetic protocol was used to introduce electron-donor substitution and aryl systems with extended π-conjugation. The dyes with the most potent electron donors show typical ICT behavior, including solvatofluorochromism and red-shifted emission with quantum yields of up to 0.4. The separated *M*- and *P*-enantiomers yield the observation of mirror-imaged ECD and CPL spectra with dissymmetry factors in the range of *ca.* 10^{-3}. Interestingly, the dyes with the most pronounced ICT character in the excited state have dissymmetry factors of about one order of magnitude smaller. The herein realized study highlights the importance of electronic factors on chiroptical dye properties and expands the platform of borylated arylisoquinolines. Further improvements may be eventually feasible by enhancing the rigidity of the dyes.

Conflicts of interest

There are no conflicts to declare.

Acknowledgements

References

1 R. Carr, N. H. Evans and D. Parker, Lanthanide complexes as chiral probes exploiting circularly polarized luminescence, *Chem. Soc. Rev.*, 2012, **41**, 7673–7686.

2 J. M. Han, S. Guo, H. Lu, S. J. Liu, Q. Zhao and W. Huang, Recent Progress on Circularly Polarized Luminescent Materials for Organic Optoelectronic Devices, *Adv. Opt. Mater.*, 2018, **6**, 1800538.

3 B. Kunnen, C. Macdonald, A. Doronin, S. Jacques, M. Eccles and I. Meglinski, Application of circularly polarized light for non-invasive diagnosis of cancerous tissues and turbid tissue-like scattering media, *J. Biophotonics*, 2015, **8**, 317–323.

4 M. Lindemann, G. Xu, T. Pusch, R. Michalzik, M. R. Hofmann, I. Žutić and N. C. Gerhardt, Ultrafast spin-lasers, *Nature*, 2019, **568**, 212–215.

5 L. E. MacKenzie and R. Pal, Circularly polarized lanthanide luminescence for advanced security inks, *Nat. Rev. Chem.*, 2021, **5**, 109–124.

6 T. Novikova, A. Pierangelo, S. Manhas, A. Benali, P. Validire, B. Gayet and A. D. Martino, The origins of polarimetric image contrast between healthy and cancerous human colon tissue, *Appl. Phys. Lett.*, 2013, **102**, 241103.

7 H. Wang, L. Liu and C. Lu, CPLC: Visible Light Communication based on Circularly Polarized Light, *Procedia Comput. Sci.*, 2018, **131**, 511–519.

8 Y. Liu, Q. Xu, J. Sun, L. Wang, D. He, M. Wang and C. Yang, Insights for vibronic effects on spectral shapes of electronic circular dichroism and circularly polarized luminescence of aza[7]helicene, *Spectrochim. Acta, Part A*, 2020, **239**, 118475.

9 G. Longhi, E. Castiglioni, J. Koshoubu, G. Mazzeo and S. Abbate, Circularly Polarized Luminescence: A Review of Experimental and Theoretical Aspects, *Chirality*, 2016, **28**, 696–707.

10 C. Schaack, L. Arrico, E. Sidler, M. Gorecki, L. Di Bari and F. Diederich, Helicene Monomers and Dimers: Chiral Chromophores Featuring Strong Circularly Polarized Luminescence, *Chem. – Eur. J.*, 2019, **25**, 8003–8007.

11 H. Tanaka, M. Ikenosako, Y. Kato, M. Fujiki, Y. Inoue and T. Mori, Symmetry-based rational design for boosting chiroptical responses, *Commun. Chem.*, 2018, **1**, 38.

12 K. Tani, R. Imafuku, K. Miyanaga, M. E. Masaki, H. Kato, K. Hori, K. Kubono, M. Taneda, T. Harada, K. Goto, F. Tani and T. Mori, Combined Experimental and Theoretical Studies on Planar Chirality of Partially Overlapped C2-Symmetric [3.3](3,9)Dicarbazolophanes, *J. Phys. Chem. A*, 2020, **124**, 2057–2063.

850 | *Org. Chem. Front.*, 2024, **11**, 843–853

This journal is © the Partner Organisations 2024

13 B. Doistau, J. R. Jimenez and C. Piguet, Beyond Chiral Organic (p-Block) Chromophores for Circularly Polarized Luminescence: The Success of d-Block and f-Block Chiral Complexes, *Front. Chem.*, 2020, **8**, 555.

14 J. R. Jimenez, M. Poncet, S. Miguez-Lago, S. Grass, J. Lacour, C. Besnard, J. M. Cuerva, A. G. Campana and C. Piguet, Bright Long-Lived Circularly Polarized Luminescence in Chiral Chromium(III) Complexes, *Angew. Chem., Int. Ed.*, 2021, **60**, 10095–10102.

15 F. Zinna and L. Di Bari, Lanthanide Circularly Polarized Luminescence: Bases and Applications, *Chirality*, 2015, **27**, 1–13.

16 D. Di Nuzzo, C. Kulkarni, B. Zhao, E. Smolinsky, F. Tassinari, S. C. J. Meskers, R. Naaman, E. W. Meijer and R. H. Friend, High Circular Polarization of Electroluminescence Achieved via Self-Assembly of a Light-Emitting Chiral Conjugated Polymer into Multidomain Cholesteric Films, *ACS Nano*, 2017, **11**, 12713–12722.

17 Y. Geng, A. Trajkovska, S. W. Culligan, J. J. Ou, H. M. P. Chen, D. Katsis and S. H. Chen, Origin of Strong Chiroptical Activities in Films of Nonafluorenes with a Varying Extent of Pendant Chirality, *J. Am. Chem. Soc.*, 2003, **125**, 14032–14038.

18 L. Wan, J. Wade, F. Salerno, O. Arteaga, B. Laidlaw, X. Wang, T. Penfold, M. J. Fuchter and A. J. Campbell, Inverting the Handedness of Circularly Polarized Luminescence from Light-Emitting Polymers Using Film Thickness, *ACS Nano*, 2019, **13**, 8099–8105.

19 L. Wan, J. Wade, X. Shi, S. Xu, M. J. Fuchter and A. J. Campbell, Highly Efficient Inverted Circularly Polarized Organic Light-Emitting Diodes, *ACS Appl. Mater. Interfaces*, 2020, **12**, 39471–39478.

20 Y. Yang, R. C. da Costa, D.-M. Smilgies, A. J. Campbell and M. J. Fuchter, Induction of Circularly Polarized Electroluminescence from an Achiral Light-Emitting Polymer via a Chiral Small-Molecule Dopant, *Adv. Mater.*, 2013, **25**, 2624–2628.

21 D. W. Zhang, M. Li and C. F. Chen, Recent advances in circularly polarized electroluminescence based on organic light-emitting diodes, *Chem. Soc. Rev.*, 2020, **49**, 1331–1343.

22 F. Zinna, U. Giovanella and L. D. Bari, Highly Circularly Polarized Electroluminescence from a Chiral Europium Complex, *Adv. Mater.*, 2015, **27**, 1791–1795.

23 F. Zinna, M. Pasini, F. Galeotti, C. Botta, L. Di Bari and U. Giovanella, Design of Lanthanide-Based OLEDs with Remarkable Circularly Polarized Electroluminescence, *Adv. Funct. Mater.*, 2017, **27**, 1603719.

24 J. Han, P. Duan, X. Li and M. Liu, Amplification of Circularly Polarized Luminescence through Triplet-Triplet Annihilation-Based Photon Upconversion, *J. Am. Chem. Soc.*, 2017, **139**, 9783–9786.

25 J. Han, D. Yang, X. Jin, Y. Jiang, M. Liu and P. Duan, Enhanced Circularly Polarized Luminescence in Emissive Charge-Transfer Complexes, *Angew. Chem., Int. Ed.*, 2019, **58**, 7013–7019.

26 A. Homberg, E. Brun, F. Zinna, S. Pascal, M. Górecki, L. Monnier, C. Besnard, G. Pescitelli, L. Di Bari and J. Lacour, Combined reversible switching of ECD and quenching of CPL with chiral fluorescent macrocycles, *Chem. Sci.*, 2018, **9**, 7043–7052.

27 L. Ji, Y. Sang, G. Ouyang, D. Yang, P. Duan, Y. Jiang and M. Liu, Cooperative Chirality and Sequential Energy Transfer in a Supramolecular Light-Harvesting Nanotube, *Angew. Chem., Int. Ed.*, 2019, **58**, 844–848.

28 J. Wade, J. R. Brandt, D. Reger, F. Zinna, K. Y. Amsharov, N. Jux, D. L. Andrews and M. J. Fuchter, 500-Fold Amplification of Small Molecule Circularly Polarised Luminescence through Circularly Polarised FRET, *Angew. Chem., Int. Ed.*, 2021, **60**, 222–227.

29 D. Yang, P. Duan and M. Liu, Dual Upconverted and Downconverted Circularly Polarized Luminescence in Donor-Acceptor Assemblies, *Angew. Chem., Int. Ed.*, 2018, **57**, 9357–9361.

30 T. Zhao, J. Han, P. Duan and M. Liu, New Perspectives to Trigger and Modulate Circularly Polarized Luminescence of Complex and Aggregated Systems: Energy Transfer, Photon Upconversion, Charge Transfer, and Organic Radical, *Acc. Chem. Res.*, 2020, **53**, 1279–1292.

31 F. Zinna, E. Brun, A. Homberg and J. Lacour, in *Circularly Polarized Luminescence of Isolated Small Organic Molecules*, ed. T. Mori, Springer Singapore, Singapore, 2020, pp. 273–292. DOI: 10.1007/978-981-15-2309-0_12.

32 L. Arrico, L. Di Bari and F. Zinna, Quantifying the Overall Efficiency of Circularly Polarized Emitters, *Chem. – Eur. J.*, 2021, **27**, 2920–2934.

33 Y. Nagata and T. Mori, Irreverent Nature of Dissymmetry Factor and Quantum Yield in Circularly Polarized Luminescence of Small Organic Molecules, *Front. Chem.*, 2020, **8**, 448.

34 J. R. Brandt, F. Salerno and M. J. Fuchter, The added value of small-molecule chirality in technological applications, *Nat. Rev. Chem.*, 2017, **1**, 0045.

35 J. R. Brandt, X. Wang, Y. Yang, A. J. Campbell and M. J. Fuchter, Circularly Polarized Phosphorescent Electroluminescence with a High Dissymmetry Factor from PHOLEDs Based on a Platinahelicene, *J. Am. Chem. Soc.*, 2016, **138**, 9743–9746.

36 S. Feuillastre, M. Pauton, L. Gao, A. Desmarchelier, A. J. Riives, D. Prim, D. Tondelier, B. Geffroy, G. Muller, G. Clavier and G. Pieters, Design and Synthesis of New Circularly Polarized Thermally Activated Delayed Fluorescence Emitters, *J. Am. Chem. Soc.*, 2016, **138**, 3990–3993.

37 J. Gilot, R. Abbel, G. Lakhwani, E. W. Meijer, A. P. H. J. Schenning and S. C. J. Meskers, Polymer Photovoltaic Cells Sensitive to the Circular Polarization of Light, *Adv. Mater.*, 2010, **22**, E131–E134.

38 P. Josse, L. Favereau, C. Shen, S. Dabos-Seignon, P. Blanchard, C. Cabanetos and J. Crassous, Enantiopure versus Racemic Naphthalimide End-Capped Helicenic Non-fullerene Electron Acceptors: Impact on Organic

This journal is © the Partner Organisations 2024

Org. Chem. Front., 2024, **11**, 843–853 | **851**

Photovoltaics Performance, *Chem. – Eur. J.*, 2017, **23**, 6277–6281.

39 M. Schulz, M. Mack, O. Kolloge, A. Lutzen and M. Schiek, Organic photodiodes from homochiral l-proline derived squaraine compounds with strong circular dichroism, *Phys. Chem. Chem. Phys.*, 2017, **19**, 6996–7008.

40 Y. Yang, R. C. da Costa, M. J. Fuchter and A. J. Campbell, Circularly polarized light detection by a chiral organic semiconductor transistor, *Nat. Photonics*, 2013, **7**, 634–638.

41 C.-H. Chen and W.-H. Zheng, Planar Chiral B–N Heteroarenes Based on [2.2]Paracyclophane as Circularly Polarized Luminescence Emitters, *Org. Lett.*, 2021, **23**, 5554–5558.

42 R. Clarke, K. L. Ho, A. A. Alsimaree, O. J. Woodford, P. G. Waddell, J. Bogaerts, W. Herrebout, J. G. Knight, R. Pal, T. J. Penfold and M. J. Hall, Circularly Polarised Luminescence from Helically Chiral "Confused" N,N,O,C-Boron-Chelated Dipyrromethenes (BODIPYs), *ChemPhotoChem*, 2017, **1**, 513–517.

43 K. Dhbaibi, L. Favereau and J. Crassous, Enantioenriched Helicenes and Helicenoids Containing Main-Group Elements (B, Si, N, P), *Chem. Rev.*, 2019, **119**, 8846–8953.

44 F. Full, Q. Wölflick, K. Radacki, H. Braunschweig and A. Nowak-Król, Enhanced Optical Properties of Azaborole Helicenes by Lateral and Helical Extension, *Chem. – Eur. J.*, 2022, **28**, e202202280.

45 J. Full, S. P. Panchal, J. Götz, A.-M. Krause and A. Nowak-Król, Modular Synthesis of Organoboron Helically Chiral Compounds: Cutouts from Extended Helices, *Angew. Chem., Int. Ed.*, 2021, **60**, 4350–4357.

46 X. Jia, J. Nitsch, L. Ji, Z. Wu, A. Friedrich, F. Kerner, M. Moos, C. Lambert and T. B. Marder, Triarylborane-Based Helical Donor–Acceptor Compounds: Synthesis, Photophysical, and Electronic Properties, *Chem. – Eur. J.*, 2019, **25**, 10845–10857.

47 H.-W. Li, M. Li, Z.-H. Zhao, C.-F. Chen, Q. Peng and C.-H. Zhao, Propeller Configuration Flipping of the Trivalent Boron-Inducing Substituent Dependence of the Circularly Polarized Luminescence Sign in Triarylborane-Based [7]Helicenes, *Org. Lett.*, 2021, **23**, 4759–4763.

48 A. Macé, K. Hamrouni, E. S. Gauthier, M. Jean, N. Vanthuyne, L. Frédéric, G. Pieters, E. Caytan, T. Roisnel, F. Aloui, M. Srebro-Hooper, B. Carboni, F. Berrée and J. Crassous, Circularly Polarized Fluorescent Helicene-Boranils: Synthesis, Photophysical and Chiroptical Properties, *Chem. – Eur. J.*, 2021, **27**, 7959–7967.

49 D. Pecorari, E. Giuliani, A. Mazzanti, S. Stagni, V. Fiorini, G. Vigarani, F. Zinna, G. Pescitelli and M. Mancinelli, Synthesis and Stereodynamic and Emission Properties of Dissymmetric Bis-Aryl Carbazole Boranes and Identification of a CPL-Active B–C Atropisomeric Compound, *J. Org. Chem.*, 2023, **88**, 871–881.

50 C. Shen, M. Srebro-Hooper, M. Jean, N. Vanthuyne, L. Toupet, J. A. Williams, A. R. Torres, A. J. Riives, G. Muller, J. Autschbach and J. Crassous, Synthesis and Chiroptical Properties of Hexa-, Octa-, and Deca-azaborahe-

licenes: Influence of Helicene Size and of the Number of Boron Atoms, *Chem. – Eur. J.*, 2017, **23**, 407–418.

51 D. Volland, J. Niedens, P. T. Geppert, M. J. Wildervanck, F. Full and A. Nowak-Król, Synthesis of a Blue-Emissive Azaborathia[9]helicene by Silicon-Boron Exchange from Unusual Atropisomeric Teraryls, *Angew. Chem., Int. Ed.*, 2023, **62**, e202304291.

52 K. Yuan, D. Volland, S. Kirschner, M. Uzelac, G. S. Nichol, A. Nowak-Król and M. J. Ingleson, Enhanced N-directed electrophilic C–H borylation generates BN–[5]- and [6]helicenes with improved photophysical properties, *Chem. Sci.*, 2022, **13**, 1136–1145.

53 F. Zhang, F. Rauch, A. Swain, T. B. Marder and P. Ravat, Efficient Narrowband Circularly Polarized Light Emitters Based on 1,4-B,N-embedded Rigid Donor–Acceptor Helicenes, *Angew. Chem., Int. Ed.*, 2023, **62**, e202218965.

54 J. Jimenez, C. Diaz-Norambuena, S. Serrano, S. C. Ma, F. Moreno, B. L. Maroto, J. Banuelos, G. Muller and S. de la Moya, BINOLated aminostyryl BODIPYs: a workable organic molecular platform for NIR circularly polarized luminescence, *Chem. Commun.*, 2021, **57**, 5750–5753.

55 J. Jiménez, F. Moreno, B. L. Maroto, T. A. Cabreros, A. S. Huy, G. Muller, J. Bañuelos and S. de la Moya, Modulating ICT emission: a new strategy to manipulate the CPL sign in chiral emitters, *Chem. Commun.*, 2019, **55**, 1631–1634.

56 E. M. Sánchez-Carnerero, A. R. Agarrabeitia, F. Moreno, B. L. Maroto, G. Muller, M. J. Ortiz and S. de la Moya, Circularly Polarized Luminescence from Simple Organic Molecules, *Chem. – Eur. J.*, 2015, **21**, 13488–13500.

57 E. M. Sánchez-Carnerero, F. Moreno, B. L. Maroto, A. R. Agarrabeitia, M. J. Ortiz, B. G. Vo, G. Muller and S. d. l. Moya, Circularly Polarized Luminescence by Visible-Light Absorption in a Chiral O-BODIPY Dye: Unprecedented Design of CPL Organic Molecules from Achiral Chromophores, *J. Am. Chem. Soc.*, 2014, **136**, 3346–3349.

58 Z. Domínguez, R. López-Rodríguez, E. Álvarez, S. Abbate, G. Longhi, U. Pischel and A. Ros, Azabora[5]helicene Charge-Transfer Dyes Show Efficient and Spectrally Variable Circularly Polarized Luminescence, *Chem. – Eur. J.*, 2018, **24**, 12660–12668.

59 V. F. Pais, M. M. Alcaide, R. López-Rodríguez, D. Collado, F. Nájera, E. Pérez-Inestrosa, E. Álvarez, J. M. Lassaletta, R. Fernández, A. Ros and U. Pischel, Strongly Emissive and Photostable Four-Coordinate Organoboron N,C Chelates and Their Use in Fluorescence Microscopy, *Chem. – Eur. J.*, 2015, **21**, 15369–15376.

60 F. Boscá, M. C. Cuquerella, V. F. Pais, A. Ros and U. Pischel, Excited-State Pathways of Four-Coordinate N,C-Chelate Organoboron Dyes, *ChemPhotoChem*, 2018, **2**, 34–41.

61 Y. Jin, Y. Makida, T. Uchida and R. Kuwano, Ruthenium-Catalyzed Chemo- and Enantioselective Hydrogenation of Isoquinoline Carbocycles, *J. Org. Chem.*, 2018, **83**, 3829–3839.

852 | *Org. Chem. Front.*, 2024, **11**, 843–853

This journal is © the Partner Organisations 2024

62 J. G. Sun, X. Y. Zhang, H. Yang, P. Li and B. Zhang, Highly Regioselective Isoquinoline Synthesis via Nickel–Catalyzed Iminoannulation of Alkynes at Room Temperature, *Eur. J. Org. Chem.*, 2018, 4965–4969.

63 R. Campos-González, P. Vázquez-Domínguez, P. Remón, F. Nájera, D. Collado, E. Pérez-Inestrosa, F. Boscá, A. Ros and U. Pischel, Bis-borylated arylisoquinoline-derived dyes with a central aromatic core: towards efficient fluorescent singlet-oxygen photosensitizers, *Org. Chem. Front.*, 2022, **9**, 4250–4259.

64 Z. Domínguez, V. F. Pais, D. Collado, P. Vázquez-Domínguez, F. N. Albendín, E. Pérez-Inestrosa, A. Ros and U. Pischel, π-Extended Four-Coordinate Organoboron N, C-Chelates as Two-Photon Absorbing Chromophores, *J. Org. Chem.*, 2019, **84**, 13384–13393.

65 D. Casarini, C. Coluccini, L. Lunazzi and A. Mazzanti, Ring Inversion Dynamics of Derivatives of Thianthrene Di- and Tetraoxide, *J. Org. Chem.*, 2006, **71**, 6248–6250.

66 M. Lin, L. Bian, Q. Chen, H. Xu, Z. Liu and K. Zhu, Cyclization of an Achiral Flipping Panel to Homochiral Tubes Exhibiting Circularly Polarized Luminescence, *Angew. Chem., Int. Ed.*, 2023, **62**, e202303035.

67 T. Yang, A. Valavalkar, A. Romero-Arenas, A. Dasgupta, P. Then, A. Chettri, C. Eggeling, A. Ros, U. Pischel and B. Dietzek-Ivanšić, Excited-State Dynamics in Borylated Arylisoquinoline Complexes in Solution and in cellulo, *Chem. – Eur. J.*, 2023, **29**, e202203468.

68 H. Tanaka, Y. Inoue and T. Mori, Circularly Polarized Luminescence and Circular Dichroisms in Small Organic Molecules: Correlation between Excitation and Emission Dissymmetry Factors, *ChemPhotoChem*, 2018, **2**, 386–402.

69 A. D. Laurent, C. Adamo and D. Jacquemin, Dye chemistry with time-dependent density functional theory, *Phys. Chem. Chem. Phys.*, 2014, **16**, 14334–14356.

70 S. Chibani, A. D. Laurent, B. Le Guennic and D. Jacquemin, Improving the Accuracy of Excited-State Simulations of BODIPY and Aza-BODIPY Dyes with a Joint SOS-CIS(D) and TD-DFT Approach, *J. Chem. Theory Comput.*, 2014, **10**, 4574–4582.